# A Novel Method for Synthesis of Titania Nanotube Powders using Rapid Breakdown Anodization

Narges F. Fahim*,†,‡ and Tohru Sekino†

*Institute of Multidisciplinary Research for Advanced Materials (IMRAM), Tohoku University, Katahira 2-1-1, Aoba-ku, Sendai 980-8577, Miyagi Pref., Japan, and Institute of Scientific and Industrial Research (ISIR), Osaka University, 8-1 Mihogaoka, Ibaraki, Osaka 567-0047-Japan*

*Received February 12, 2009. Revised Manuscript Received March 23, 2009*

The present paper describes a new method utilizing rapid anodization to quickly synthesize high-quality, high aspect ratio, robust titanium dioxide nanotube powders. $TiO_2$ nanotube powders, with a typical nanotube outer diameter of approximately 40 nm, wall thickness of approximately 8−15 nm, and length of about 10−35 $\mu$m, were synthesized by potentiostatic rapid breakdown anodization of titanium foils in aqueous electrolytes of 0.3 M NaCl or 0.1 M $HClO_4$ under an applied potential of 20 V. High reactivity and ultrahigh reaction rate are cornerstones responsible for periodic release of $TiO_2$ nanotubes into solution and formation of a white precipitate of $TiO_2$ nanotubes. The reaction yield is approximately 4−6 g in less than 3 h, and the approximate cost of the material is $3.50/g, based on the laboratory-scale production. Various characterization techniques, including FESEM, HRTEM, EDX, XRD, XPS, FT-IR, UV−visible diffuse-reflectance, and $N_2$ adsorption, have been used to probe morphology, microstructure, crystallographic, composition, bond configuration, optical properties, and surface area of the nanotubes. XPS and EDX investigations show that nanotubes formed in NaCl/phosphate electrolyte solutions contain a significant amount of phosphorus species, which strongly affects crystallization and phase transformation of $TiO_2$. Namely, phosphate-incorporating nanotubes stabilized the anatase phase, and initiation of the rutile phase was observed at annealing temperatures ≥700 °C. The resulting nanotube powders have a significant level of OH groups with a band gap ranging from 3.04 to 3.23 eV. Our results indicate that rapid breakdown anodization is highly efficient in the production of good-quality $TiO_2$ nanotube powders, which makes it an alternative to well-documented conventional methods.

## 1. Introduction

Titanium dioxide ($TiO_2$), or titania, is of great interest for a number of technological areas, including heterogeneous catalysis, photocatalysis, photovoltaic solar cells, gas sensors, waste remediation, batteries, photonic crystals, ultraviolet blockers, smart coating, and filling materials in textiles, paints, paper, and cosmetics, as well as biomedical science, because of its electronic, optoelectronic, catalytic, and biocompatibility properties coupled with its low cost and chemical stability. Titania is a wide band gap semiconductor has great ability to produce powerful oxidants (holes in the valence band) and reductants (electrons in the conduction band) by absorbing photons.[1,2] Because of this feature and its mechanical strength, $TiO_2$ has been widely studied for applications in photoelectrochemical systems, such as $TiO_2$ photoanodes for dye-sensitized photovoltaic solar cells and in water-splitting for hydrogen generation.[3−5]

Exponential growth of research activities has been seen in nanoscience and nanotechnology in the past decades. One-dimensional $TiO_2$ nanostructures, such as nanotubes, nanowires, and nanobelts, have attracted much attention in recent years, because new physical and chemical properties emerge when the size of the material becomes smaller and smaller, down to the nanometer scale. The motion of electrons and holes in semiconductor nanomaterials is primarily governed by the well-known quantaum confinement, and transport properties related to phonons and phonons are largely affected by the size and geometry of the materials.[6] Surface area and surface-to-volume ratio increase dramatically as the size of material particles decreases.[7] A high surface area associated with a small particle size is very beneficial in many $TiO_2$-based devices, and their performance is largely influenced by the size of $TiO_2$ building units. For example, titania nanotubes have shown a more than 2-fold increase in the short-circuit current density compared to nanoparticles in thin film dye-sensitized solar cells.[8] Titania nanotubes also provide channels for enhanced electron transfer, thereby helping to increase the efficiency of solar cells, as well as the efficiency of electrolysis and photocatalysis.

* Corresponding author. Tel: +81-6-6879-8451. Fax: +81-6-6875-8454. E-mail: fnarges@hotmail.com, narges15@sanken.osaka-u.ac.jp.
† Tohoku University.
‡ Osaka University.

(1) Stone, V. F.; Davis, R. J. *Chem. Mater.* **1998**, *10*, 1468.
(2) Adachi, M.; Murata, Y.; Harada, M.; Yoshikawa, S. *Chem. Lett.* **2000**, *29*, 942.
(3) O'Regan, B.; Grä tzel, M. *Nature (London)* **1991**, *353*, 737.
(4) Park, N. G.; Lagemaat, J.; Frank, A. J. *J. Phys. Chem. B* **2000**, *104*, 8989.
(5) Khan, S. U. M.; Al-Shahry, M.; Ingler, W. B. *Science* **2002**, *297*, 2243.
(6) Burda, C.; Chen, X.; Narayanan, R.; El-Sayed, M. A. *Chem. Rev.* **2005**, *105*, 1025.
(7) Chen, X.; Lou, Y.; Dayal, S.; Qiu, X.; Krolicki, R.; Burda, C.; Zhao, C.; Becker, J. *Nanosci. Nanotechnol.* **2005**, *5*, 1408.
(8) Adachi, M.; Murata, Y.; Okada, I.; Yoshikawa, S. *J. Electrochem. Soc.* **2003**, *150*, G488.

10.1021/cm900410x CCC: $40.75 
Published on Web 04/17/2009

Titania nanotubes of various sizes have been synthesized by different groups using techniques such as anodization,[9−15] hydrothermal synthesis,[16−20] template-based synthesis,[21,22] sol−gel,[23] and molecular assembly.[8] Anodic oxidation continues to excite interest since Zwillang et al. in 1999[24] successfully prepared $TiO_2$ nanotubes on a Ti surface. There has been growing interest in the synthesis of titania nanotubes by anodization due to the simplicity of materials preparation and handling, as well as more control over the synthesis process as compared to other methods. In conventional routes, a multistep process is required and materials preparation is comparatively complex (long process, high temperatures). Over the past few years, much progress has been achieved in fabrication of self-organized $TiO_2$ nanotube layers using anodization in fluoride-containing solutions.[25−27] In the latter case, anodization for many hours in nonaqueous electrolytes is required to form long nanotubes. Another recently proposed electrochemical approach to very rapidly (within seconds) form high aspect ratio nanotube bundles on Ti is anodization of Ti under breakdown conditions in chloride- or perchlorate-containing electrolytes.[28−37] It is interesting to note that nanotube bundles obtained by rapid breakdown anodization (RBA) show significantly higher photoresponse and conversion efficiencies than tubes formed under self-ordering conditions.[38] In our previous work, such nanotube bundles grown by RBA and doped with silica particles show very promising osseointegrative properties when used as a bioactive material for hydroxyapatite growth.[39]

However, most of the work has been focused on anodization of titanium foils to generate nanotube bundles on Ti surfaces. Application of such a material architecture in functional devices is limited due to the following: (a) the presence of an opaque Ti foil underneath a nanostructure in certain applications of optical-electrical devices (e.g., dye-sensitized solar cells) requires backside illumination that reduces the light-to-electrical energy conversion because of the platinized counter electrode partially reflects light and iodine in the electrolyte absorbs photons in the near UV region, and (b) the presence of a titanium metal underneath nanotubes may result in an electrical short-circuit when they are utilized in devices. Therefore, there is a pressing need to fabricate high aspect ratio $TiO_2$ nanotubes in a form that can be applied for a variety of functional substrates for various technological applications. Moreover, Grimes and co-workers[40] anodized titanium thin films/FTO glass and used them in a front-side dye-sensitized solar cell. They found conversion efficiencies of 2.9% from a 360-nm thick nanotube film. The method demonstrated by Grimes's group enables the front side illumination, but with a limited thickness (300−500 nm).

Still, a low-cost fabrication of titanium oxide nanostructures of high quality with controllable properties is a significant and ongoing challenge within nanoscience and nanotechnology. In addition, continuing breakthroughs in synthesis and modification of $TiO_2$ nanomaterials have brought new properties and new applications with improved performance. However, to the best of the authors' knowledge, up to now there have been no reports on the synthesis of a powder form of $TiO_2$ nanotube (NT) bundles by electrochemical anodization. Due to the low structural stability of $TiO_2$ NTs at high temperatures, it is of significant importance to investigate how the tubular structure and crystalline phases would vary with subsequent annealing. This study demonstrates a novel, one-step method based on an electrochemical approach, namely, rapid breakdown anodization, which quickly leads to synthesis of high aspect ratio titania nanotubes in a powder form. $TiO_2$ nanotube powders have been typically formed by electrochemical oxidation of titanium foils in an electrolyte containing chloride or perchlorate ions. Morphological, structural, and optical


(9) Gong, D.; Grimes, C. A.; Varghese, O. K.; Hu, W.; Singh, R. S.; Chen, Z.; Dickey, E. C. *J. Mater. Res.* **2001**, *16*, 3331.
(10) Ghicov, A.; Tsuchiya, H.; Macak, J. M.; Schmuki, P. *Electrochem. Commun.* **2005**, *7*, 505.
(11) Tsuchiya, H.; Macak, J. M.; Ghicov, A.; Taveira, L.; Schmuki, P. *Corros. Sci.* **2005**, *47*, 3324.
(12) Tsuchiya, H.; Macak, J. M.; Taveira, L.; Balaur, E.; Ghicov, A.; Sirotna, K.; Schmuki, P. *Electrochem. Commun.* **2005**, *7*, 576.
(13) Tsuchiya, H.; Macak, J. M.; Taveira, L.; Schmuki, P. *Chem. Phys. Lett.* **2005**, *410*, 188.
(14) Mor, G. K.; Varghese, O. K.; Paulose, M.; Grimes, C. A. *Adv. Funct. Mater.* **2005**, *15*, 1291.
(15) Varghese, O. K.; Gong, D.; Paulose, M.; Grimes, C. A.; Dickey, E. C. *J. Mater. Res.* **2003**, *18*, 156.
(16) Kasuga, T.; Hiramatsu, M.; Hoson, A.; Sekino, T.; Niihara, K. *Langmuir* **1998**, *14*, 3160–3163.
(17) Kasuga, T.; Hiramatsu, M.; Hoson, A.; Sekino, T.; Niihara, K. *Adv. Mater.* **1999**, *11*, 1307.
(18) Zhang, S. L.; Zhou, J. F.; Zhang, Z. J.; Du, Z. L.; Vorontsov, A. V.; Jin, Z. S. *Chin. Sci. Bull.* **2000**, *16*, 1533.
(19) Zhang, Q. H.; Gao, L. A.; Sun, J.; Zheng, S. *Chem. Lett.* **2002**, *2*, 226.
(20) Yao, B. D.; Chan, Y. F.; Zhang, X. Y.; Zhang, W. F.; Yang, Z. Y.; Wang, N. *Appl. Phys. Lett.* **2003**, *82*, 281–283.
(21) Hoyer, P. *Adv. Mater.* **1996**, *8*, 857.
(22) Liu, S. M.; Gan, L. M.; Liu, L. H.; Zhang, W. D.; Zeng, H. C. *Chem. Mater.* **2002**, *14*, 1391.
(23) Lei, Y.; Zhang, L. D.; Meng, G. W.; Li, G. H.; Zhang, X. Y.; Liang, C. H.; Chen, W.; Wang, S. X. *Appl. Phys. Lett.* **2001**, *78*, 1125.
(24) Zwilling, V.; Darque-Ceretti, E.; Boutry-Forveille, A.; David, D.; Perrin, M. Y.; Aucouturier, M. *Surf. Interface Anal.* **1999**, *27*, 629.
(25) Ruan, C.; Paulose, M.; Varghese, O. K.; Mor, G. K.; Grimes, C. A. *J. Phys. Chem. B* **2005**, *109*, 15754.
(26) Mac'ak, J. M.; Tsuchiya, H.; Schmuki, P. *Angew. Chem., Int. Ed.* **2005**, *44*, 2100.
(27) Mac'ak, J. M.; Tsuchiya, H.; Taveira, L.; Aldabergerova, S.; Schmuki, P. *Angew. Chem., Int. Ed.* **2005**, *44*, 1.
(28) Fahim, N. F.; Sekino, T.; Morks, M. F.; Kusunose, T. J. *Nanosci. Nanotechnol.* **2009**, *9*, 1803.
(29) Hahn, R.; Macak, J. M.; Schmuki, P. *Electrochem. Commun.* **2007**, *9*, 947.
(30) Nakayama, K.; Kubo, T.; Asano, T.; Tsubokura, A.; Nishikitani, Y. In *Proceedings of the 208th ECS Meeting*; 2005; Abstract #819 and Abstract #843.
(31) Allam, N. K.; Grimes, C. A. *J. Phys. Chem. C* **2007**, *111*, 13028.
(32) Panaitescu, E.; Richter, C.; Menon, L. *J. Electrochem. Soc.* **2008**, *155*, E7.
(33) Nakayama, K.; Kubo, T.; Nishikitania, Y. *Electrochem. Solid-State Lett.* **2008**, *11*, C23−C26.
(34) Ishibashi, K.; Yamaguchi, R.; Kimura, Y.; Niwanoa, M. *J. Electrochem. Soc.* **2008**, *155* (1)), K10.
(35) Nguyen, Q. A.; Bhargava, Y. V.; Devine, T. M. *Electrochem. Commun.* **2008**, *10*, 471.
(36) Richter, C.; Panaitescu, E.; Willey, R.; Menona, L. *J. Mater. Res.* **2007**, *22*, 1624.
(37) Richter, C.; Wu, Z.; Panaitescu, E.; Willey, R. J.; Menon, L. *Adv. Mater.* **2007**, *19*, 946.
(38) Hahn, R.; Stergiopoulus, T.; Macak, J. M.; Tsoukleris, D.; Kontos, A. G.; Albu, S. P.; Kim, D.; Ghicov, A.; Kunze, J.; Falaras, P.; Schmuki, P. *Phys. Status Solidi (RRL)* **2007**, *1*, 135.
(39) Fahim, N. F.; Morks, M. F.; Sekino, T. *Electrochim. Acta* **2009**, *54*, 3255.
(40) Mor, G. K.; Shankar, K.; Paulose, M.; Varghese, O. K.; Grimes, C. A. *Nano Lett.* **2006**, *6*, 215.

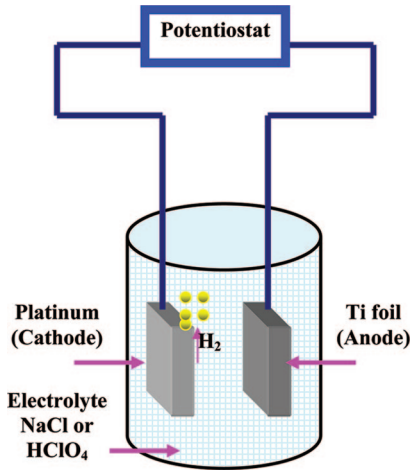


**Figure 1.** Schematic diagram of the anodization setup.

properties of powders were studied. Transitions between $TiO_2$ phases upon heat treatment and their thermal stability have also been thoroughly examined.

## 2. Materials and Methods

**2.1. Materials.** Ti foils (99.5% purity, 0.1 mm thickness) were purchased from Nilaco Corp. and, before anodization, cleaned by sonicating in acetone, 2-propanol, and methanol, followed by rinsing with deionized (DI) water and drying in a nitrogen stream. The electrolytes were NaCl or $HClO_4$ purchased from Sigma Aldrich, and all the solutions were prepared from reagent-grade chemicals and deionized water.

**2.2. Methods.** *2.2.1. $TiO_2$ Nanotubes Powder Preparation.* Pieces (5 cm × 5 cm) were punched out from a stock Ti foil. As-prepared pieces were clamped into a Cu clip and immersed directly in electrolytes. In this study, two kinds of electrolytes were used; electrolyte A consisted of 0.3 M NaCl buffered with 0.3 M $NH_4H_2PO_4$ to pH 4.4 (the powder produced in this electrolyte is denoted as powder A); and electrolyte B was composed of 0.1 M $HClO_4$ (the powder prepared in this electrolyte is denoted as powder B). Anodization was performed in a two-electrode configuration with a titanium foil as a working electrode and a platinum foil as a counter electrode, under a constant potential of 20 V at a temperature of approximately 25 °C. A computer-monitored potentiostat (Model AMEL 7050) was employed to control the potential and record the current, as shown in Figure 1. Electrochemical treatment consisted of a potential stepping from an open-circuit potential (OCP) to 20 V in one step followed by maintaining the applied potential at 20 V for less than 1 h for each piece until the initial foil was completely transformed into $TiO_2$ nanotube powder. Afterward, the as-grown $TiO_2$ nanotube powder (white precipitate) was washed several times with DI water, collected by centrifugation, filtered, and finally oven-dried at 60 °C overnight. Eventually, a white powder was obtained as seen in the photographic image in Figure 2. In order to produce well-defined crystalline structures, all powders were annealed for 3 h in air with a heating rate of 30 °C/min using Advantec KM-100 electric muffle furnaces. Powder A was annealed at 480, 550, 600, and 700 °C, while powder B was annealed at 480 °C to compare structures of powders that were produced in different electrolytes. This fabrication process and its steps are summarized in a schematic diagram shown in Figure 2. Another set of experiments was performed to investigate the effect of bath temperature (25, 37, 7, 3 °C) and stirring on the morphology of the resulting nanotubes.

*2.2.2. $TiO_2$ Nanotubes Powder Characterization.* All the powders (as-grown and annealed) were characterized by a number of different methodologies, including field-emission scanning electron microscope (SEM), high resolution transmission electron microscopy (HRTEM), selected area electron diffraction (SAED), energy dispersive X-ray spectroscopy (EDX), X-ray diffraction (XRD), X-ray photoelectron spectroscopy (XPS), Fourier-transform infrared spectroscopy (FT-IR), diffuse reflectance UV−visible spectroscopy, and $N_2$ adsorption/desorption isotherms.

*Electron Microscopy.* Size, morphology, and chemical composition of as-grown and annealed $TiO_2$ powders were initially characterized using a field emission SEM (FESEM) (Hitachi S-5000, Tokyo, Japan, with EDX capabilities) at accelerating voltages of 20 kV. Specifically, nanostructured $TiO_2$ powders were mounted onto conductive carbon tapes, which were then attached onto the surfaces of SEM brass stubs. These samples were then coated with Au/Pd by sputtering for 10 s to minimize charging effects under SEM imaging conditions. HRTEM images and SAED patterns were obtained (Hitachi, H-8100) at an accelerating voltage of 200 kV to further characterize the morphologies of individual nanostructures and to confirm the nanotubular structural as well as the nature of $TiO_2$ films, whether crystalline or amorphous. Specimens for the TEM investigations were prepared by depositing a drop of these suspension solutions of $TiO_2$ nanotube powder onto a 300 mesh Cu grid, coated with a holey carbon film. Prior to deposition, a small quantity of powders in ethanol was sonicated for 20 min to ensure adequate dispersion in solution.

*X-ray Diffraction (XRD).* Crystallographic, crystallinity, and purity information was recorded by X-ray diffraction using a powder X-ray diffractometer (Rigaku RINT 2500, Tokyo, Japan) with Cu Kα radiation ($\lambda = 1.54$ Å) at 40 kV and 50 mA with a scan rate of 0.02°/s and a scan speed of 1°/min over a $2\theta$ range from 10° to 90°. The resulting XRD spectra were compared with titania (anatase and rutile; JCPS No. 21-1272 and JCPS No. 21-1276, respectively), and sodium titanate ($Na_2Ti_5O_{11}$, card No. 11-289). The crystallite size of anatase $TiO_2$ has been estimated from the broadening of the diffraction line of the (101) plane at 25.4° by using the Scherrer equation [$D = K\lambda/(\beta \cos \theta)$],[41] where $K$ is a dimensionless constant that depends on the crystallite shape but is assumed to be constant ($K = 0.89$). $\lambda$ is the X-ray wavelength ($\lambda = 0.154\,06$ nm for Cu Kα), $\theta$ is the diffraction angle, and $\beta$ is the full-width at half-maximum (fwhm) of the (101) plane (in radians).

*X-ray Photoelectron Spectroscopy (XPS).* The composition and chemical state of various species present in samples were determined by using X-ray photoelectron spectroscopy (ESCALAB 220i system, Fisons Instruments, Al Kα: 1486.6 eV). The X-ray source was operated at 10 kV and 10 mA; survey and high-resolution spectra were acquired at a pass energy of 25 eV and a take-off angle of 35°. The unresolved XPS peaks were decomposed into subcomponents using a Gaussian (85%)−Lorentzian (15%) curve fitting program and a Shirley-type baseline. The X-ray photoelectron spectra were referenced to a C1s peak ($E_b \sim 285.2$ eV) resulting from an adventitious hydrocarbon present on the sample surface (i.e., from the XPS instrument itself).

(41) Scherrer, P. *Gottinger Nachrichte* **1918**, *2*, 98.

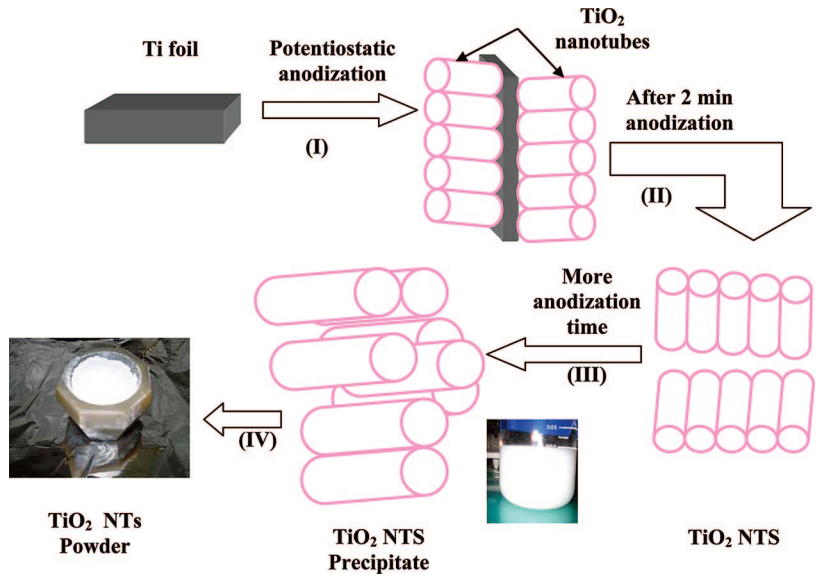


**Figure 2.** Schematic diagram showing the fabrication process of $TiO_2$ NT powders obtained via potentiostatic rapid breakdown anodization. (I) $TiO_2$ NT bundles are synthesized on both sides of Ti foil; (II) after anodization for more than 2 min, due to the vigorous nature and the ultrahigh speed of the reaction, the tubes formed on the Ti surface start releasing into the electrolyte; (III) the anodization process continues until the initial Ti metal foil is completely transformed into $TiO_2$ NTs and a white precipitate has been formed; (IV) the precipitated $TiO_2$ NTs are thoroughly washed with distilled $H_2O$, centrifuged, filtered, and finally dried in an oven at 60 °C overnight. Photographs show the final appearance of $TiO_2$ NT powder obtained by the rapid breakdown anodization method.

*Fourier-Transform Infrared Spectroscopy (FT-IR).* Spectra were measured in transmission mode using a KBr technique at a resolution of 4 $cm^{-1}$ with sample scans equal to 300 and recorded in the range from 4000 to 400 $cm^{-1}$ using a JASCO 4100 spectrometer. Powders were mixed with KBr and then pressed into transparent pellets with a diameter of 10 mm using a hydraulic press at a pressure of 100 $kg/cm^2$.

*Diffuse-Reflectance UV−visible Spectroscopy.* Diffuse-reflectance UV−visible spectra for evaluation of absorption properties were recorded in the diffuse-reflectance mode (*%R*) and transformed to absorbance spectra using the Kubelka−Munk model.[42,43] The spectra were recorded on a JASCO-570 spectrophotometer equipped with an integrating sphere; $BaSO_4$ was used as a standard. The band-gap energy of $TiO_2$ NT powders can be estimated from the Kubelka−Munk absorption spectra by calculating an absorption coefficient, $\alpha$.

Semiconductors absorb light below a threshold wavelength, the fundamental absorption edge, which is related to the band gap energy ($E_g$) via[44]

$$E_g\,(\mathrm{eV}) = 1240/\lambda_g\,(\mathrm{nm}) \qquad (1)$$

For a direct band gap transition of titanium dioxide, the absorption coefficient ($\alpha$) is related to the photon energy ($E_{ph}$) via[45]

$$(E_{ph}\alpha) = B(E_{ph} - E_g)^{0.5} \qquad (2)$$

From the Tauc's plot of $(E_{ph}\alpha)^{0.5}$ vs $E_{ph}$, the band gap energy can be determined by extrapolating the linear region to $\alpha = 0$ so that the intercept of the line with the horizontal axis gives the absorption energy that corresponds to the band gap energy.

*$N_2$ Adsorption.* The pore structure of the obtained $TiO_2$ nanotube powders was characterized by $N_2$ adsorption using an adsorption apparatus (Quantachrome NOVA Instruments V 2.2 gas sorption analyzer). Surface area of the samples was determined from the Brunauer−Emmett−Teller (BET) equation, and pore volume was determined from the total amount adsorbed at relative pressures near unity.

## 3. Results and Discussion

**3.1. Synthesis of $TiO_2$ Nanotube Powders.** The first set of experiments was conducted to monitor growth of $TiO_2$ nanotube powders with use of the two kinds of solutions. Anodizing solutions were either 0.1 M $HClO_4$ or 0.3 M NaCl/$NH_4H_2PO_4$. Anodization was performed at an anodization voltage of 20 V and at room temperature (25 °C). The second set of anodization experiments was carried out in a NaCl electrolyte to examine the effect of various anodization parameters such as bath temperature (37, 25, 7, 3 °C) and stirring on nanotube morphology and on reaction rate. Also, an anodization experiment was performed under magnetic stirring, and it was found that magnetic stirring can reduce the synthesis time by up to 50%. Moreover, conducting an anodization experiment with two counter electrodes instead of one reduced the synthesis time by more than 50% (i.e., increased the reaction rate). These findings are in good agreement with results from Schumki and co-workers.[29]

Figure 3 shows the current−time behavior observed during potentiostatic anodization of Ti foils in (a) 0.1 M $HClO_4$ and (b) 0.3 M NaCl buffered to pH 4.3 with 0.3 M $NH_4H_2PO_4$ electrolytes at an anodization voltage of 20 V. It is apparent that anodization occurs under current flow >1 A

(42) Orel, Z. C.; Gunde, M. K.; Orel, B. *Prog. Org. Coat.* **1997**, *30*, 59.
(43) An, T.; Zhu, X.; Xiong, Y. *Chemosphere* **2002**, *46*, 897.
(44) Gratzel, M. *Heterogeneous Photochemical Electron Transfer*; CRC Press: Boca Raton, FL, 1988.
(45) Pankove, J. I. *Optical Processes in Semiconductors*; Dover: New York, 1971; Chapter 3.

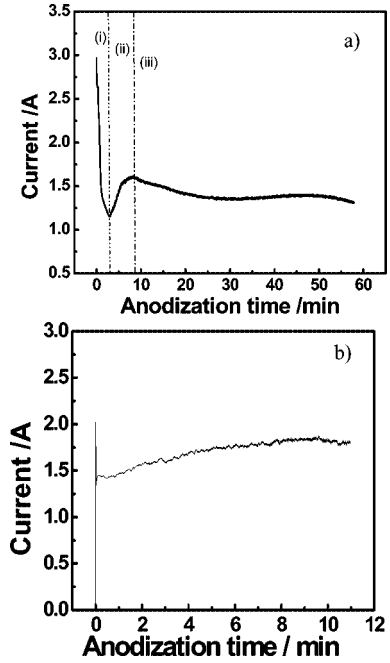


**Figure 3.** The current−time behavior observed during preparation of $TiO_2$ nanotube powders by rapid breakdown anodization at 20 V in (a) 0.1 M $HClO_4$ and (b) 0.3 M $NaCl/NH_4H_2PO_4$ electrolytes.

for anodization of Ti in electrolyte containing chloride or perchlorate ions. Obviously, the current plot exhibits three distinct regions: (i) an initial abrupt exponential decay followed by (ii) a region of rising current and then (iii) a region where the current becomes steady with a little decrease. The corresponding current−time trend visible in Figure 3 is essentially identical to that seen when nanotube bundles are formed on the surface of a Ti foil.[28] The difference in reaction rates is confirmed by the current versus time plots in Figure 3. It can be seen that the current reaches a steady state within 1 min when anodizing in the NaCl electrolyte, compared with ∼10 min when anodizing in the $HClO_4$ electrolyte. The steady state of the current vs time indicates development of repassivation and saturation of nanotube formation.

Formation mechanism of $TiO_2$ nanotubes can be explained in the light of the current−time plots, as follows. Initially, titanium oxidizes to form a compact layer of $TiO_2$ via the reaction

$$Ti + 2H_2O \rightarrow TiO_2 + 4H^+ + 4e^- \text{ (at the anode)} \quad (3)$$

This oxide layer leads to a dramatic decrease in the recorded current due to its poor electrical conductivity. It is interesting to note that the current decreased drastically within a few seconds (Figure 3, region i). After that, $TiO_2$ starts to dissolve, forming pores and leading to the observed slight increase in the current (Figure 3, region ii). This can be explained as follows. At sufficiently higher voltages (producing a strong electric field for breakdown of the $TiO_2$ pacifying layer), chlorine inhibits growth of the pacifying oxide layer, which results in inward migration of oxygen atoms, and oxidation of titanium is maintained. Simultaneously, titanium atoms at the electrolyte/oxide interface can be swept away through dissolution with chlorine species (i.e., chlorine enhances cation dissolution). Although $TiO_2$ is thermodynamically stable within the pH range 2−12, a complexing ligand (Cl) leads to a significant dissolution. The mechanism of pit formation due to Cl ions is described by the following equation:

$$TiO_2 + 6Cl^- \rightarrow [TiCl_6]^{2-} + 2H_2O \quad (4)$$

This is supported by the high stability of the $[TiCl_6]^{2-}$ complex, with its free energy of formation ranging from −5.12 to −10.90 kcal/mol, depending on the cation type.[46] Finally, a steady state of the current (plateau region) and the growth of nanotubes in length are achieved (Figure 3, region iii). A rapid evolution of hydrogen at the cathode is observable as strong bubbling of the reaction vessel due to a reaction

$$4H^+ + 4e^- \rightarrow 2H_2\uparrow \text{ (at the cathode)} \quad (5)$$

Fabrication of $TiO_2$ nanotube powders by rapid breakdown anodization is summarized in Figure 2 and involves four steps: (I) $TiO_2$ NT bundles are synthesized on both sides of Ti foil; (II) after anodization for more than 2 min, due to the vigorous nature and the ultrahigh speed of the reaction, tubes formed on the Ti surface start releasing into the electrolyte; (III) the anodization process continues until the initial Ti metal foil is completely transformed into $TiO_2$ NTs, and a white precipitate has been formed; and (IV) the precipitated $TiO_2$ NTs are thoroughly washed with distilled $H_2O$, centrifuged, filtered, and finally dried in an oven at 60

**Table 1. Synthesis and Morphological Characteristics of the $TiO_2$ Nanotube Powders Prepared by Rapid Breakdown Anodization Method[a]**

| | | | | morphology | | | | |
|---|---|---|---|---|---|---|---|---|
| sample | synthesis conditions | crystal polymorphism | crystallite sizes, $d_{XRD}$ (nm) | o.d. (nm) | wall thickness (nm) | length ($\mu$m) | $S_{BET}$ ($m^2/g$) | $E_{bg}$ (eV) |
| powder A | anodized in 0.3 M NaCl/0.3 M $NH_4H_2PO_4$ electrolyte, pH 4.4 and at 20 V | | | 22−42 | 8−15 | 10−35 | | |
| powder A-as | as-grown | amorphous | | | | | − | 3.09 |
| powder A-480 °C | annealed at 480 °C | anatase | 10.44 | | | | 58 | 3.13 |
| powder A-550 °C | annealed at 550 °C | anatase | 12.77 | | | | − | 3.18 |
| powder A-600 °C | annealed at 600 °C | anatase | 14.9 | | | | − | 3.23 |
| powder A-700 °C | annealed at 700 °C | anatase + rutile | 20.11 | | | | − | 3.09 |
| powder B | anodized in 0.1 M $HClO_4$ electrolyte pH 1.39 and at 20 V | | | 40 | 8−15 | 20−25 | | |
| powder B-as | as-grown | amorphous | | | | | − | 3.13 |
| powder B-480 °C | annealed at 480 °C | anatase + rutile | 13 | | | | 74 | 3.04 |

[a] Data obtained by SEM, TEM, XRD, and UV−vis spectroscopy.

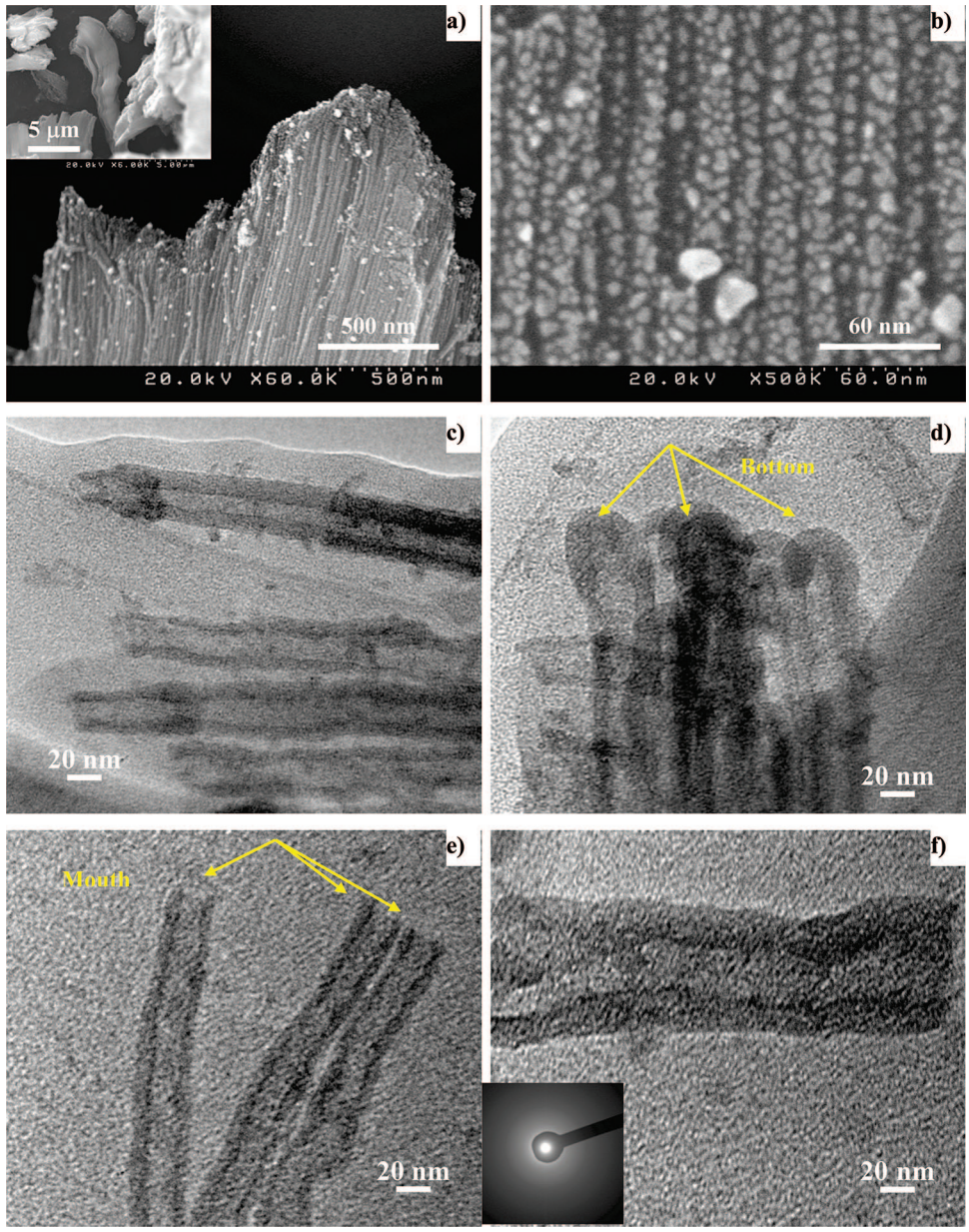


**Figure 4.** As-grown titania nanotube powder synthesized in $HClO_4$ electrolyte at 20 V. (a, b) Typical FESEM images at two different magnifications; the inset shows the length of the as-formed $TiO_2$ powder. (c−f) HRTEM images show the nanotubular structure of the resulting $TiO_2$ nanotube powder with open mouth and closed bottom, as well as the tube wall. (The particles observed in SEM images are due to Au/Pd coating for SEM observation.)

°C overnight. Photographs show the final appearance of $TiO_2$ NT powder obtained by the rapid breakdown anodization method. Formation of $TiO_2$ nanotube powder by this kind of anodization can be explained as follows. The ultrarapid reaction allows no time for relaxation of the processes and adjustment of the increased volume associated with the nanotube formation. Areas containing nanotubes experience a vigorous explosion of the material, probably due to local mechanical stress imposed by surrounding areas, which do not allow any significant increase in volume associated with nanotube formation. Consequently, the result is a periodic release of nanotubes into solution. This means that the reaction rate and solution reactivity are factors responsible for release of $TiO_2$ nanotubes in solution and formation of $TiO_2$ nanotube powder.

This method can provide a convenient, rapid, one-step, alternative route for production of titanium oxide nanotube powders, which are now routinely synthesized by a hydrothermal method.[16−20]This method also leads to optimal usage of titanium foil accompanied by rapid formation of large quantities of titanium oxide powders (about 4−6 g in less than 3 h). Finally, we note that, at the laboratory scale of production, the approximate cost of nanotube powders is $3.50/g. Synthesis conditions and various morphological and structural characteristics of titanium oxide nanotube powders prepared via rapid breakdown anodization are tabulated in Table 1. These powders are intended to be used in dye-sensitized solar cells as photoanodes by coating FTO glass with them to form transparent $TiO_2$ NTs photoanodes, which can enable front side illumination with controllable thickness.

(46) Chassaing, E.; Basile, F.; Lorthioir, G. *J. Less-Common Met.* **1979**, *68*, 153.

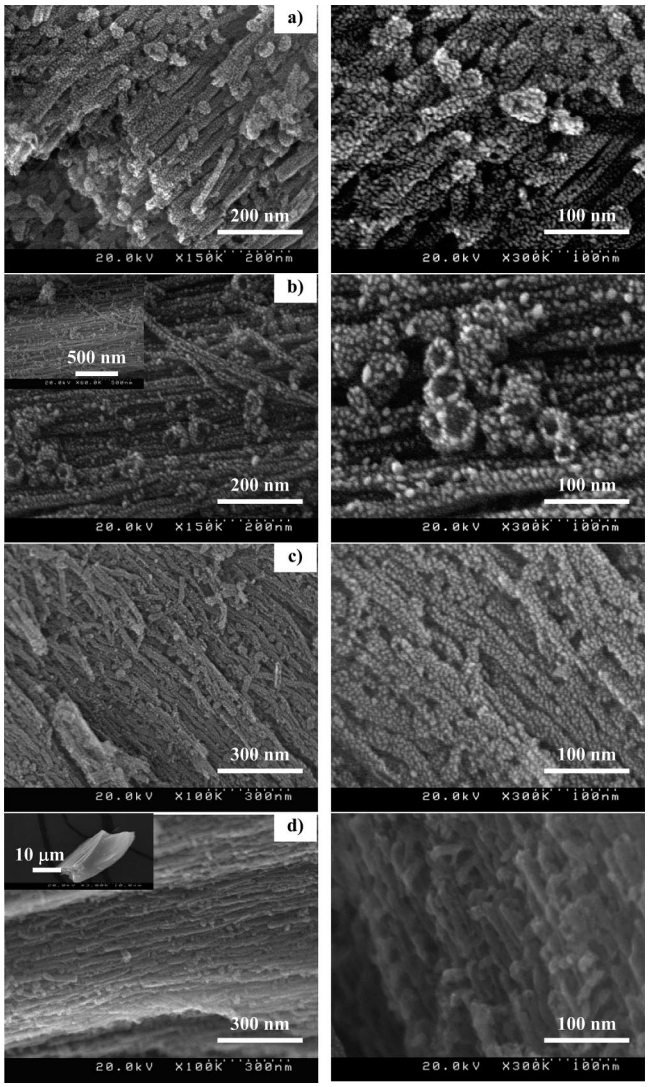


**Figure 5.** FESEM micrographs of as-grown titania nanotube powder synthesized in NaCl buffered with phosphate solution, pH 4.4, at different experimental conditions of stirring and bath temperature: (a) at 25 °C with stirring of 470 rpm (top view), (b) at 7 °C, (c) at 37 °C, and (d) at 25 °C (room temperature) side view.

**3.2. $TiO_2$ Nanotubes Powder Characterization.** *3.2.1. Morphological and Microstructural Properties.* Figure 4a,b shows typical SEM images of the side and close-up top view of a nanotube powder prepared in $HClO_4$ electrolyte by rapid breakdown anodization. The tubes are well-ordered and grow very rapidly in dense bundles of approximately 20−25 $\mu$m in length. HRTEM images of the as-grown nanotube powder are shown in Figure 4c−f. The images indicate a nanotubular structure of the as-grown powder with a nanotube outer diameter (o.d.) of about 40 nm, inner diameter (i.d.) in the range 10−15 nm, and a wall thickness of ∼8−15 nm (Figure 4d−f). A bundle of perfect tubes with smooth surface can be seen in Figure 4c. Amorphous nature of the nanotube structure is confirmed by SAED patterns taken from different parts of the nanotubes (Figure 4f). The diffraction pattern shows several broad diffuse rings expected for the amorphous state. Both HRTEM and XRD data (Figures 4f and 9) demonstrate that the as-grown high aspect ratio $TiO_2$ nanotube powder has an amorphous structure.

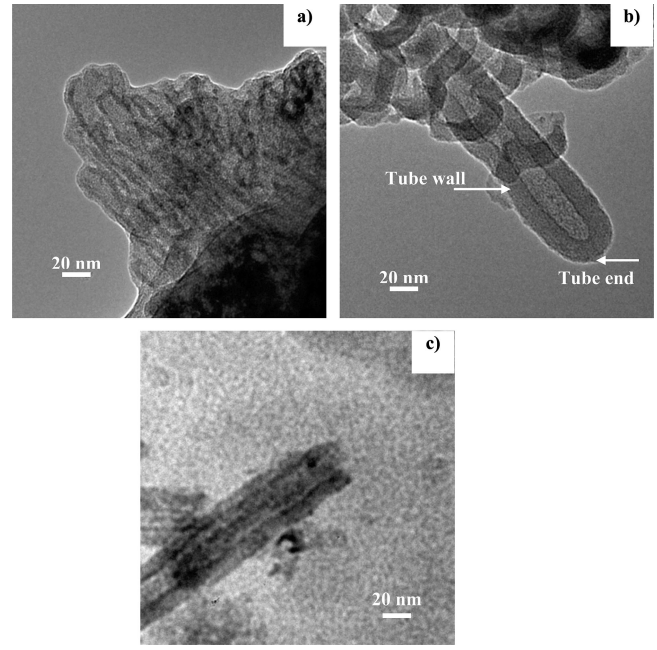


**Figure 6.** HRTEM images of as-grown titania nanotube powder synthesized in NaCl electrolyte at different bath temperature of (a) 37 °C, (b) 7 °C, and (c) 3 °C.

Figure 5 shows FESEM images of as-grown $TiO_2$ nanotube powders synthesized in NaCl/phosphate solutions at different anodization conditions (stirring and bath temperatures). Several images showing various morphologies and orientations of nanotubes are presented in Figure 5. These images indicate that the $TiO_2$ powders consist of highly ordered nanotubes with lengths in the range of 10−35 $\mu$m and with aspect ratios of ∼454−875 (the inset in Figure 5d). On the basis of our observations (Figure 4), no discernible changes in the nanotubular morphology or dimensions were found when the anodization was carried out at different anodization parameters of temperatures and stirring. HRTEM was used to get insight into the microstructure of the titania nanotube powder on the atomic level. HRTEM images (Figure 6a−c) support that the as-grown titania powder consists of nanotube bundles with smooth surfaces that can keep their shape without damage when separating them for the TEM imaging. Also, it is evident that pore mouths are open on the top of the layer, while on the bottom of the structure the tubes are closed. HRTEM observations revealed that these nanotubes have o.d. of ∼22−42 nm, i.d. of 10−20 nm, and a wall thicknesses of about 8−15 nm (Figure 6a−c), in line with results reported in the literature.[28−37] The average nanotube dimensions calculated from SEM and TEM images are in a good agreement. There were no significant morphological differences between titania nanotubes fabricated at different temperatures. Our data about the effect of bath temperature on the morphology and dimensions of $TiO_2$ NTs are in good agreement with that mentioned by Wang and Lin.[47] On the contrary, Grimes and co-workers[48] studied the effect of bath temperature on the dimensions of $TiO_2$ NTs grown in fluoride-containing electrolyte, and they found that

(47) Wang, J.; Lin, Z. J. *Phys. Chem. C* **2009**, *113*, 4026.
(48) Mor, G.; Shankar, K.; Paulose, M.; Varghese, O.; Grimes, C. *Nano Lett.* **2005**, *5*, 191.

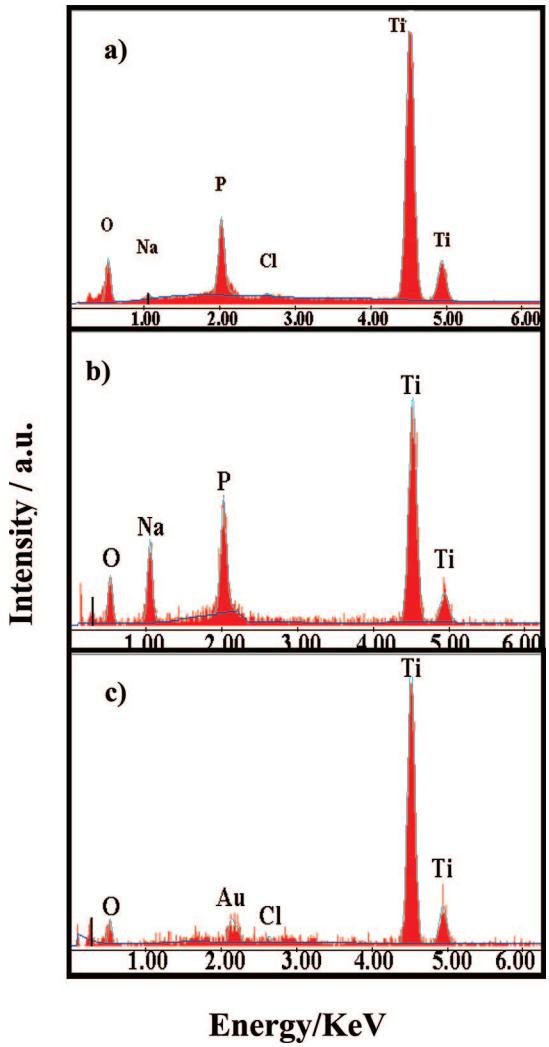


**Figure 7.** EDX spectra of $TiO_2$ nanotube powders synthesized by RBA in different electrolytes: (a) 0.3 M NaCl, as-grown, (b) 0.3 M NaCl, annealed at 700 °C, and (c) 0.1 M $HClO_4$, annealed at 480 °C. These spectra show that powder) contains sodium and phosphorus impurities, while powder B contains only Ti, O, and a trace of Cl ions.

both the length and wall thickness were affected by bath temperature: at 5 °C, length = 224 nm and wall thickness = 34 nm, while at 50 °C, length = 120 nm and wall-thickness = 9 nm.

*3.2.2. Elemental Analysis and Chemical States.* Figure 7 shows typical EDX spectra from nanotube powders synthesized by the rapid breakdown anodization (RBA) at 20 V in different electrolytes of (a) 0.3 M NaCl, as-grown, (b) 0.3 M NaCl, annealed at 700 °C, and (c) 0.1 M $HClO_4$, annealed at 480 °C. Obviously, sodium and phosphorus peaks are seen in the EDX spectra for the powder obtained by anodization in the NaCl electrolyte (Figure 7a,b). The sodium peak intensity increased after annealing at a high annealing temperature (700 °C) due to crystallization of sodium titanate at annealing temperatures >600 °C.[49] This is in good agreement with the presence of sodium titanate peaks in the XRD spectra (Figure 9a). The Cl peak completely disappeared after annealing at 700 °C. The spectrum for powder B, synthesized in $HClO_4$, contains major peaks due to Ti and O and a minor peak due to traces of Cl (Figure 7c). Thus, we conclude that powder B is purer than powder A.

Figure 8 shows XPS spectra of a titania nanotube powder that was prepared in 0.3 M NaCl electrolyte and annealed at 480 °C in air for 3 h. XPS survey spectrum (Figure 8a) reveals that the $TiO_2$ powder consists mainly of 54.5 atom % of oxygen and 36 atom % of titanium. The rest are negligible traces of Na at 1071.9 eV (1.28 atom %), P at 133.6 eV (8 atom %), and Cl at 199 eV (0.24 atom %) from the electrolyte. Figure 8b displays a Ti 2p region spectrum showing the presence of the main doublet composed of two symmetrical peaks at 459.0 eV (Ti $2p^{3/2}$) and 464.7 eV (Ti $2p^{1/2}$), which can be assigned to $Ti^{4+}$ in a tetragonal structure. A high-resolution O 1s spectrum is shown in Figure 8c. The peak with a binding energy of 530.9 eV could be mainly attributed to the Ti−O in $TiO_2$. In the case of bulk $TiO_2$, oxygen was found at 530.3 eV.[50] Also, a small shoulder can be seen at a higher binding energy of 533 eV, which can be assigned to the OH groups or to chemisorbed $H_2O$ on the surface of the sample.[51] A P 2p peak was observed at 133.6 eV (Figure 8d), corresponding to $H_2PO_4^-$ or $HPO_4^{2-}$ from electrolyte solution.[52,53] It can be concluded that the powder consists of $TiO_2$. On the other hand, the $TiO_2$ powder obtained from potentiostatic anodization of Ti foil in $HClO_4$ electrolyte at 20 V is composed of O (58.3 atom %) and Ti (40.6 atom %). The rest is remnant Cl (1.1 atom %) in the tube matrix.

*3.2.3. Phases and Crystallinity.* XRD patterns of $TiO_2$ nanotube powders prepared in different electrolytes of NaCl and $HClO_4$ for as-grown and annealed at various temperatures in air for 3 h are shown in Figure 9a,b. The as-grown $TiO_2$ nanotubular powders were found to be amorphous. The intensity of the (101) peak of the thermodynamically stable anatase crystal structure grew with increase of annealing temperature for both types of nanotube powders. This indicates the improvement of the crystallization of anatase phase. The width of the main peaks becomes narrower, suggesting growth of anatase grains. An average particle size estimated from (101) crystal plane of anatase is listed in Table 1 for both types of powders. Clearly, the crystallite size is inversely related to the fwhm of an individual peak; the narrower the peak, the larger the crystallite size. As has been mentioned above, the nanotube powder prepared in the NaCl electrolyte contains sodium and phosphorus species as impurities from electrolyte. The presence of sodium titanate peaks in the spectra from powders annealed at temperatures >600 °C, as is evident from Figure 9a, indicates that annealing at these temperatures causes sodium impurities to crystallize into sodium titanate ($Na_2Ti_5O_{11}$). If annealing

(49) Poudel, B.; ZWang, W.; Dames, C.; Huang, J. Y.; Kunwar, S.; Wang, D. Z.; Banerjee, D.; Chen, G.; Ren, Z. F. *Nanotechnology* **2005**, *16*, 1935.

(50) Sodergren, S.; Siegbahn, H.; Rensmo, H.; Lindstrom, H.; Hagfeldt, A.; Lindquist, S. E. *J. Phys. Chem. B* **1997**, *101*, 3087.

(51) Yu, J. C.; Yu, J. G.; Tang, H. Y.; Zhang, L. Z. *Mater. Chem.* **2002**, *12*, 81.

(52) Wagner, C. D.; Naumkin, A. V.; Vass, A. K.; Allison, J. W.; Powell, C. J.; Rumble, J. R., Jr. NIST X-ray photoelectron Spectroscopy Database, NIST Standard Reference Database 20, version 3.4 (Web Version); http://srdata.nist.gov/xps (accessed December 2008).

(53) Wagner, C. D.; Riggs, W. M.; Davis, L. E.; Moulder, J. F. In *Handbook of X-ray Photoelectron Spectroscopy*; Mullenberg, G. E., Ed.; Perkin-Elmer: Norwalk, CT, 1979.

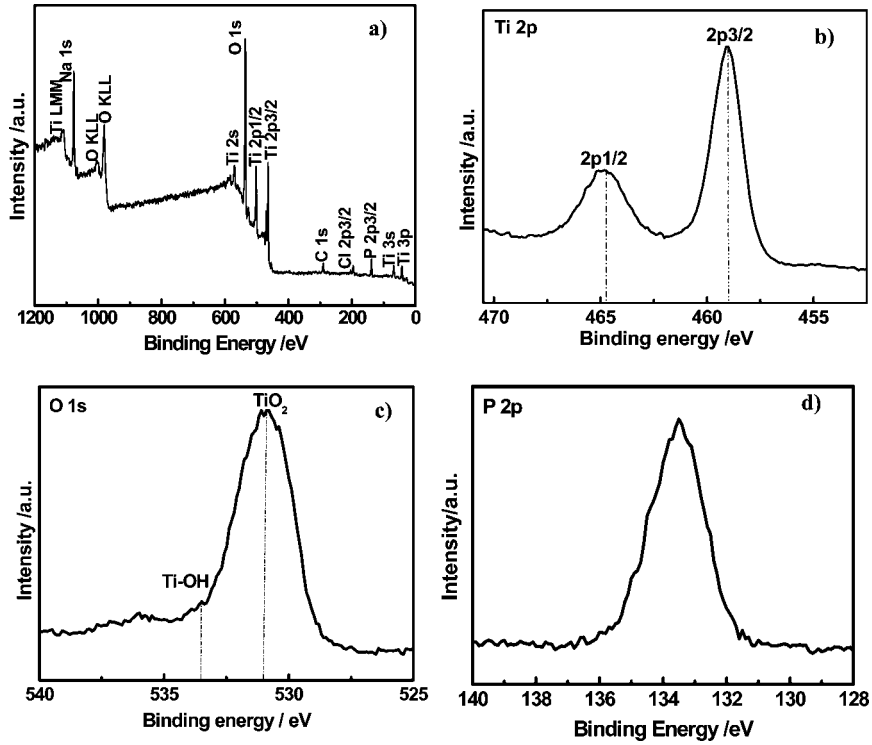


**Figure 8.** XPS spectra of $TiO_2$ nanotube powder prepared by rapid breakdown anodization of Ti foil in electrolyte (0.3 M NaCl and buffered to pH = 4.4 with 0.3 M $NH_4H_2PO_4$) at 20 V and annealed at 480 °C for 3 h in air atmosphere: (a) wide scan indicating the main peaks of Ti and O and the minor peaks corresponding to P, Na, and Cl (impurities from electrolyte), (b) Ti 2p spectrum, (c) O1s spectrum, and (d) P 2p spectrum.

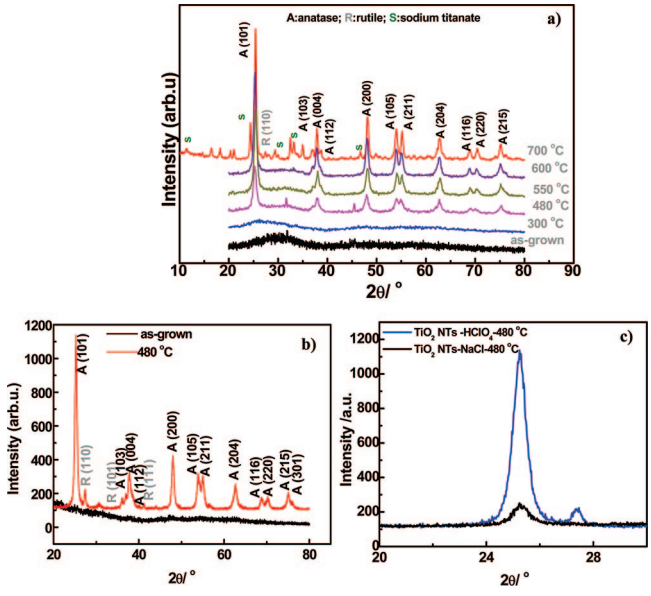


**Figure 9.** XRD patterns of $TiO_2$ nanotube powder synthesized via potentiostatic RBA at 20 V in different electrolytes: (a) 0.3 M NaCl for as-grown and annealed powders at different temperatures from 300 to 700 °C and (b) 0.1 M $HClO_4$ for as-grown and annealed powders at 480 °C. (c) Patterns showing the crystallization behavior of the two powders prepared in different electrolytes; the powder synthesized in $HClO_4$ electrolyte exhibits strong anatase peaks with the presence of rutile peak, while the powder prepared in NaCl electrolyte contains only anatase peaks (under the same annealing condition).

temperature is too low, sodium will not be able to crystallize into sodium titanate. Similar results have been observed by others.[49] As is seen from Figure 9a, the anatase phase is stable up to 600 °C (single-phase anatase), while a small peak begins to appear at an annealing temperature of 700 °C. An important observation in the XRD patterns was initiation of the rutile phase at 480 °C in the nanotubes powder prepared in the $HClO_4$ electrolyte (Figure 9b,c). No rutile initiation was observed for this annealing temperature for nanotubes prepared in the NaCl electrolyte (Figure 9a). It has been previously observed[54,55] that phosphate-incorporated titania nanotubes stabilize the anatase form of $TiO_2$ (i.e., the temperature for the anatase-to-rutile phase transition increases for titania nanotubes containing phosphate species). Therefore, the onset of rutile transformation was not observed in the phosphate-containing nanotube powder at the corresponding temperature (480 °C). Crystallite size is an important factor for stability of the crystalline phases of titania. Anatase is stable at smaller grain sizes and transforms to rutile more readily with increasing grain size.[56] Moreover, phosphate ions are known to stabilize the anatase phase of bulk titania.[57] Clearly, the anatase-to-rutile transformation temperature of 700 °C for powders obtained by anodization in NaCl is below the transformation temperature of 925 °C for a bulk nanopowder but well above the transformation temperature of ≥550 °C reported for titania nanotubes prepared by anodization.[28,58] To our surprise, the impurities in the titania nanotube powders had a strong influence on the phase formation and transition temperatures of anatase to rutile. It is interesting to note that storing as-grown

(54) Kar, P.; Raja, K. S.; Misra, M.; Agasanapur, B. N. *Mater. Res. Bull.* **2009**, *44*, 398.
(55) Criado, J.; Real, C. J. *Chem.Soc., Faraday Trans.* **1983**, *179*, 2765.
(56) Ke-rong, Z.; Ming-Sheng, Z.; Jian-Ming, H.; Zhen, Y. *Mater. Sci. Eng., A* **2005**, *403*, 87.
(57) Korosi, L.; Dekany, I. *Collids Surf. A* **2006**, *28*, 146.

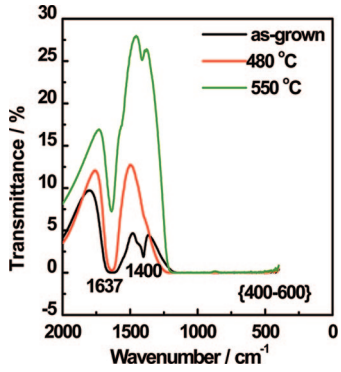


**Figure 10.** FT-IR spectra of $TiO_2$ nanotube powder A synthesized in 0.3 M NaCl electrolyte of as-grown and annealed at 480 and 550 °C.

nanotubes (amorphous phase) in an oven at 60 °C for 10 days led to crystallization with anatase as the predominant phase for both powders.

*3.2.4. Bonds Configuration and Functional Group Properties.* In order to understand what can happen in the tube structure with annealing, the bond configuration was analyzed using an FT-IR technique. Figure 10 presents FT-IR spectra of as-grown $TiO_2$ nanotube powder produced in the NaCl electrolyte, as well as of powders annealed at 480 and 550 °C. As seen in Figure 10, there were three peaks at 1637, 400−600, and 1400 $cm^{-1}$, which can be assigned to the vibrations of O−H and Ti−O bonds of $TiO_2$ nanotubes.[17] The peak around 1400 $cm^{-1}$ in the spectra is most likely attributed to the presence of phosphate species or carbon contamination in the form of $CO_3^{2-}$. A significant change in the spectra appears after annealing at 480 and 550 °C, where the intensity of the characteristic Ti−O peaks increased. This indicates a transformation from the as-formed amorphous structure to the anatase crystalline structure, in line with the result of XRD. The intensity of the OH group decreases with annealing. Nonetheless, we cannot reduce the possibility that there may be a significant amount of hydroxyl species on the surfaces of these nanotube powders, which would be beneficial for an enhanced photocatalytic activity of these materials.[59,60]

*3.2.5. Morphological and Structure Characteristics after Annealing.* Figure 11 illustrates microstructure and morphology of $TiO_2$ nanotube powder B produced by anodization in the $HClO_4$ electrolyte and annealed at 480 °C for 3 h in air. The SEM data (Figure 11a,b) clearly show that the nanotube powder can maintain its nanotubular structure, even after annealing at 480 °C for 3 h. High-resolution transmission electron microscopy (HRTEM) images of powder annealed at 480 °C are shown in Figure 11c,d. These images clearly indicate crystallization of the tube walls with an average crystallite size of ∼13 nm, in line with our XRD data. Furthermore, both XPS and EDX analyses show that annealing is accompanied by reduction of chlorine ions (as contaminant from anodization electrolyte).

Figure 12 shows different morphologies obtained as a result of annealing for powder A at annealing temperatures of 480, 550, 600, and 700 °C. FESEM micrographs (Figure 12a,b) clearly indicate that the nanotubular integrity is maintained at annealing temperatures <600 °C. On the contrary, annealing in air for 3 h at a higher temperature ≥600 °C resulted in collapse of nanotube bundles (Figure 12c). Moreover, annealing at 700 °C favors sintering and tends to destroy nanostructures completely (Figure 12d). Nanotube structure was found to be stable up to approximately 550 °C. Above this temperature, nanotubes start collapsing and being destroyed. The powder annealed at 600

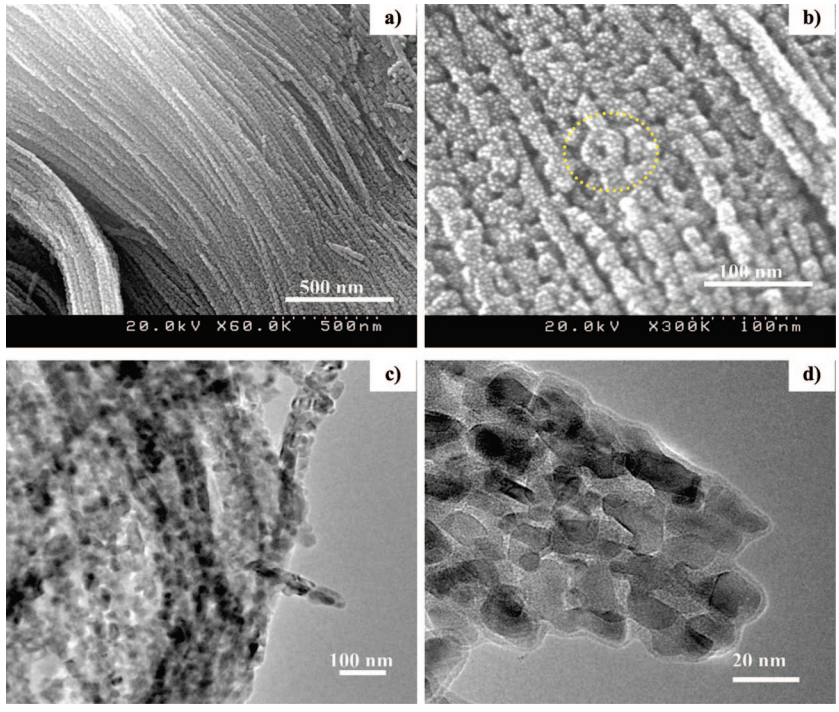


**Figure 11.** As-grown titania nanotube powder synthesized in $HClO_4$ electrolyte and annealed at 480 °C for 3 h in air atmosphere. (a, b) FESEM images at two different magnifications. (c, d) TEM and HRTEM images show the $TiO_2$ nanotube powder with crystallized walls.

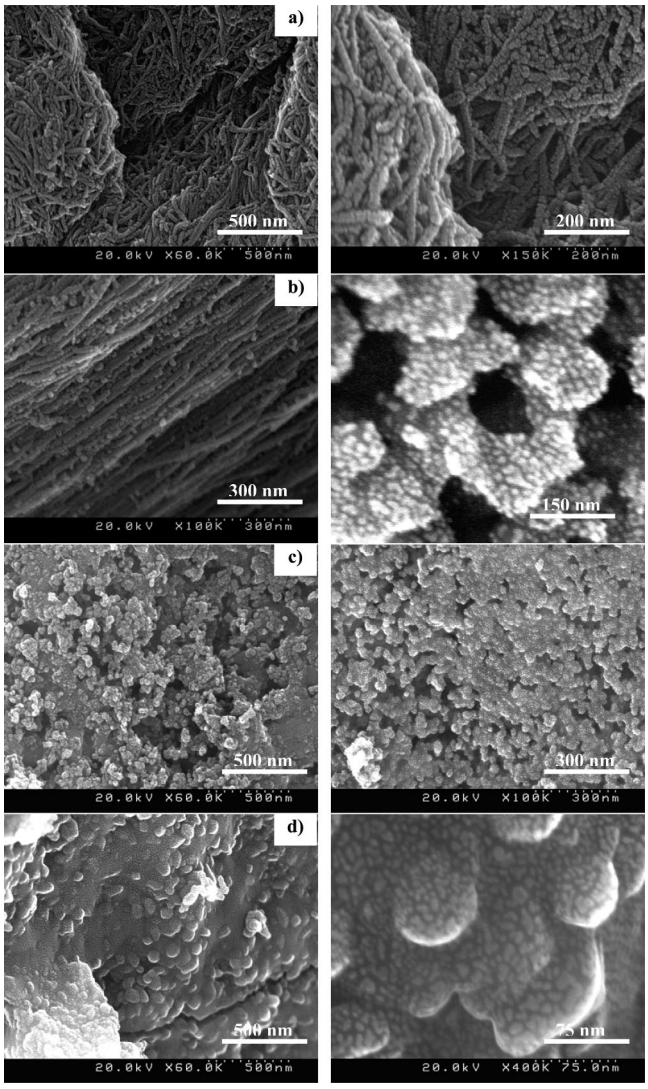


**Figure 12.** FESEM micrographs of titania nanotube powder synthesized in NaCl electrolyte and annealed in air for 3 h at (a) 480 °C, (b) 550 °C, (c) 600 °C, and (d) 700 °C.

°C (Figure 12c) has a mixed morphology, including nanotubes and spherical nanoparticles. Extended annealing in air at 700 °C for 3 h leads to more morphological changes of nanotubes.

To get a clearer picture of the influence of annealing on structure and crystalline phases of the high aspect ratio $TiO_2$ nanotube powder A, grown by RBA in NaCl electrolyte, TEM images were taken. Figure 13a−c shows high-resolution transmission electron microscope images of $TiO_2$ nanotube powder annealed at temperatures of 480, 550, and 700 °C in air for 3 h. Clearly, crystal fringes (fingerprint) can be seen that have an interplanar distance of 0.352 nm, corresponding to the *d*-spacing of the (101) lattice plane of anatase (Figure 13a−c). The nanotube powder annealed at 480 °C shows a dominant crystalline structure, as demonstrated in Figure 13a: small $TiO_2$ crystallites with a size of approximately 10 nm are present in the tube walls. However,

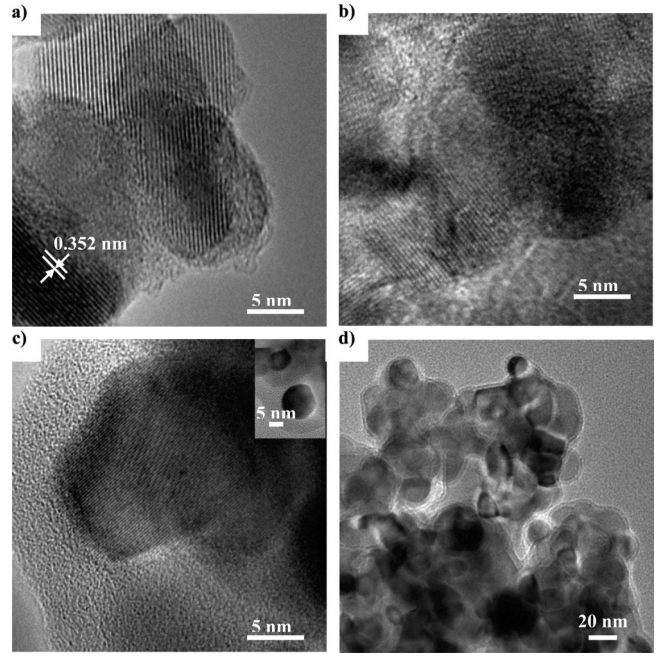


**Figure 13.** HRTEM images of $TiO_2$ nanotube powder synthesized in NaCl electrolyte and annealed in air atmosphere for 3 h at (a) 480 °C, (b) 550 C, and (c, d) 700 °C. the inset in image c shows the spherical nanoparticles after the nanotubular integrity is lost. The images show the fingerprint of the anatase crystal structure.

the average crystallites size ($d_{XRD}$) estimated from the XRD (101) peak is about 10.44 nm. On the other hand, annealing at 700 °C results in further development of anatase crystallites. Anatase crystallites become 19.5−24.5 nm in size, although there are some crystals of rutile with a size of ∼31 nm (Figure 13d). Growth of the crystalline phase with annealing observed during the HRTEM studies is consistent with changes in the XRD spectra. In other words, for the high aspect-ratio tubes investigated here, annealing at temperatures from 480 to 600 °C provokes growth of titania nanotubes with a single phase anatase structure. This experimental finding is in line with the idea of the thermodynamic stability of anatase phase in small titania crystallites (ranging from 10 to 20 nm).[61] Finally, we observed a complete transformation from pure amorphous to crystalline single phase anatase in the titania nanotube powder after annealing at 600 °C. Structural analysis shows that small crystallites with a diameter of 15 nm appear on the tube walls. It should be noted that similar morphological changes were observed by Grimes and co-workers,[15] but the phase transition temperature is slightly different. Both XRD and HRTEM measurements demonstrate that as-grown high aspect ratio $TiO_2$ nanotube powders have an amorphous structure that can be entirely transformed into anatase or a mixture of anatase and rutile by selecting a proper annealing temperature depending on the impurity content, particle size, and other parameters.

*3.2.6. Optical Properties of the Powders.* Figure 14 depicts the UV−visible diffuse-reflectance spectra and Tauc's plots for both powders A and B of as-grown and annealed titania nanotubes. It can be seen from parts a and b of Figure 14 that the maximum absorption edge for powder A, as-grown

(58) Varghese, O. K.; Gong, D.; Paulose, M.; Grimes, C. A.; Dickey, E. C. *J. Mater. Res.* **2003**, *18*, 156.
(59) Cao, L.; Huang, A.; Spiess, F.-J.; Suib, S. L. *J. Catal.* **1999**, *188*, 48.
(60) Vorontsov, A. V.; Altynnikov, A. A.; Savinov, E. N.; Kurkin, E. N. *J. Photochem. Photobiol. A* **2001**, *144*, 193.
(61) Zhang, H.; Banfield, J. *J. Mater. Chem.* **1998**, *8*, 2073.

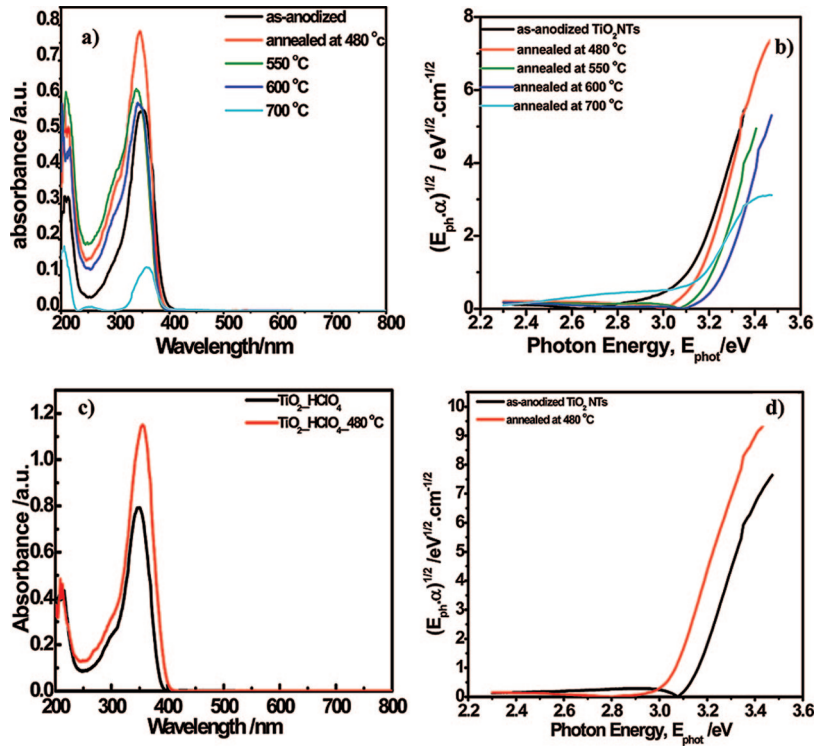


**Figure 14.** UV−visible diffuse reflectance spectra of $TiO_2$ nanotube powders synthesized by RBA in different electrolyte: (a) powder A, 0.3 M NaCl, of as-grown and annealed at 480, 550, 600, and 700 °C and (c) powder B, 0.1 M $HClO_4$, of as-grown and annealed at 480 °C (b, d) Their Tauc's plots for band gap determination.

and annealed at 480, 550, 600, and 700 °C, is at 401, 396, 389, 384, and 401 nm, respectively. Band gap energies estimated from Tauc's plots are 3.09, 3.13, 3.18, 3.23, and 3.09 eV, respectively. The band gap energy was changed under annealing temperature (increased upon annealing temperature ≤600 and then decreased at annealing temperature of 700 °C). Such behavior is attributed to the different phases of titania, where annealing at temperatures ≤600 resulted in crystallization into anatase phase of $TiO_2$ with band gap energy of 3.25 eV, while annealing at >600 °C resulted in the emergence of the rutile phase of lower band gap (3.1 eV).[62] This explanation is in good agreement with the XRD data. The absorption spectra and the band gaps are shifted to longer wavelengths and to smaller band gaps compared to bulk anatase with a maximum absorption edge at 380 nm and a band gap of 3.25 eV.[62,63] A red-shift in the as-grown powder in NaCl electrolyte may be due to incorporation of phosphorus species into the $TiO_2$ nanotubes. The P and N species introduce band gap states due to the lattice diffusion of these species during the anodization process, as reported by Raja et al.[64,65] Moreover, Asahi et al.[66] calculated the density of states (DOS) for an anatase crystal doped with carbon, nitrogen, and phosphorus and found that states introduced by carbon and phosphorus substitutions are too deep to overlap with anatase band gap. However, the increased photoactivity of carbon-doped $TiO_2$ nanotubes has been well-documented.[67,68] Similarly, incorporation of phosphorus species can be also considered a cause of the increase in the photoactivity of $TiO_2$. Incorporation of phosphate species was verified by both XPS and EDX results. The band gap energies in this work are in a good agreement with the literature data.[5] Absorbance and band gaps of as-grown and annealed $TiO_2$ nanotube powder B, prepared in $HClO_4$ electrolyte, were found to be 3.13 eV (396 nm) and 3.04 eV (408 nm), respectively, as shown in Figure 14c,d. Moreover, the absorption intensity of the annealed powder is higher than that of the as-anodized nanotube powder. Therefore, $TiO_2$ nanotubes in the anatase form are more beneficial as a photocatalytic and solar cell conversion material.

By comparing our $TiO_2$ nanotube powders with free-standing $TiO_2$ nanotube membrane[69,70] in terms of applications (e.g., photovoltaics and photocatalysis), the following can be withdrawn: first, the thickness of free-standing membrane of $TiO_2$ nanotube is usually in the range of 100−145 $\mu$m and such high thickness is not required for most applications, specially for photovoltaic solar cells[71] where the optimum thickness is in the range of 20−30 $\mu$m. Also, Jennings et al.[72] estimated the diffusion length of

(62) Chen, X.; Samuel, S. M. *Chem. Rev.* **2007**, *107*, 2891.
(63) Finklea, H. O. *Semiconductor Electrodes*; Elsevier: New York, 1988; Chapter 2.
(64) Raja, K. S.; Mahajan, V. K.; Misra, M. *J. Power Sources* **2006**, *159*, 1258.
(65) Shi, Q.; Yang, D.; Jiang, Z.; Li, J. *J. Mol. Catal. B: Enzym.* **2006**, *43*, 44.
(66) Asahi, R.; Morikawa, T.; Ohwaki, T.; Aoki, K.; Taga, Y. *Science* **2001**, *293*, 269.
(67) Li, Y.; Hwang, D.-S.; Lee, N. H.; Kim, S.-J. *Chem. Phys. Lett.* **2005**, *404*, 25.
(68) Sakthivel, S.; Kisch, H. *Angew. Chem., Int. Ed.* **2003**, *42*, 4908.
(69) Wang, J.; Lin, Z. *Chem. Mater.* **2008**, *20*, 1257.
(70) Albu, S.; Ghicov, A.; Macak, J.; Hahn, R.; Schmuki, P. *Nano Lett.* **2007**, *7*, 1286.
(71) Macak, J. M.; Tsuchiya, H.; Ghicov, A.; Yasuda, K.; Hahn, R.; Bauer, S.; Schmuki, P. *Curr. Opin. Solid State Mater. Sci.* **2007**, *11*, 3.
(72) Jennings, J. R.; Ghicov, A.; Peter, L. M.; Schmuki, P.; Walker, A. B. *J. Am. Chem. Soc.* **2008**, *130*, 13364.

photoinjected electrons in $TiO_2$ nanotube cells and they found it to be on the order of 100 $\mu$m, which greatly influences the transport of electrons when $TiO_2$ NTs are used as photoactive anode in devices. By using high aspect ratio $TiO_2$ nanotube powders, which were prepared in this study, the thickness can be controlled. Moreover, the production cost can be reduced by using $TiO_2$ NTs powders produced by RBA that formed in aqueous electrolyte in short time by a one-step method, in contrast to free-standing membrane of $TiO_2$ NTs, which requires long time (60 h) in nonaqueous electrolyte (ethylene glycol), and this issue is of significant importance for practical applications. Second, to use either $TiO_2$ NTs powders or free-standing $TiO_2$ NTs membrane in dye-sensitized solar cells, one should anchor the material to a supporting substrate such as FTO glass. Nanotube powders coated the conductive glass either by screen printing or by spin coating, while free-standing membrane can be anchored to conductive glass by using transparent conductive glue, which could increase the resistance of the cell and hence the photocurrent may be reduced. The comparison between the $TiO_2$ powders produced in this study and free-standing $TiO_2$ NTs membrane in terms of applications is an interesting subject for future work.

## 4. Conclusions

We have demonstrated for the first time a fast synthesis of titania nanotube powders by using a low-cost, simple, and convenient electrochemical rapid breakdown anodization method. $TiO_2$ nanotube powders have been typically produced by potentiostatic anodization of titanium foil in an electrolyte containing 0.3 M $NaCl/NH_4H_2PO_4$ or 0.1 M $HClO_4$ at 20 V. High reactivity and ultrahigh reaction rate are cornerstones for the periodic release of $TiO_2$ nanotubes into solutions and formation of white precipitate of $TiO_2$ nanotubes. This method results in a more efficient usage of the titanium foil and produces large quantities of $TiO_2$ nanotube powders with a reaction yield of approximately 4−6 g in less than 3 h. The approximate cost of the nanotube powders is $3.50/g based on laboratory-scale production. Our results indicate that the as-grown nanotube powder has a smooth morphology with a typical nanotube outer diameter of about 40 nm, wall thickness of approximately 8−15 nm, and length of about 10−35 $\mu$m with aspect ratios ranging from 454 to 875. The as-grown $TiO_2$ nanotube powders have an amorphous structure, which can be transformed into a crystalline structure by annealing. An additional feature of the $TiO_2$ powder formed in the NaCl/phosphate electrolyte is that phosphate ions can be incorporated into nanotubes. This modification of composition can play an important role in crystallization and phase transitions of titania nanotube powders. For powder A, formed in a 0.3 M NaCl electrolyte, single-phase anatase starts emerging upon annealing at temperatures $\leq$600 °C, and the onset of rutile at an annealing temperature of 700 °C has been observed, but morphology starts changing from nanotubes to nanoparticles above 550 °C. For powder B, produced in a 0.1 M $HClO_4$ electrolyte, rutile phase initiation was observed at 480 °C, while no rutile phase was found in the phosphate-containing nanotubes (powder A) at this temperature. Furthermore, nanotube powders produced by this method have good optical properties with band gap energy ranging from 3.04 to 3.23 eV. Finally, it can be concluded that the rapid anodization method is a highly efficient technique for fast synthesis of high aspect ratio nanotube powders with controllable properties, which may improve their performance in environmental (photocatalysts, sensors) and photovoltaic green energy (dye solar cells, water splitting for $H_2$ generation) applications. This method can also be extended to prepare doped titania nanotubes powders in an one-step process.

**Acknowledgment.** Financial support of the Japan Society for the Promotion of Science (JSPS Fellows) under Grant-in-Aid 19-07069 is gratefully acknowledged. The authors are grateful to Prof. Dr. Kobayashi and Assoc. Prof. Dr. Takahashi from FCM Laboratory, Osaka University, for their support. Helpful assistance from Dr. Seino (TEM measurements), at the Faculty of Engineering, Osaka University, is greatly acknowledged.

CM900410X